Supporting information

$(Fe_xNi_{1-x})_4N$ Nanoparticles: Magnetism and Electrocatalytic Properties for Oxygen Evolution Reaction

Structural characterization

X-ray diffraction (XRD) patterns were recorded to analyze the phase and crystal structure of the as-synthesized samples using a Shimadzu XRD-6100, operated at a step size of 0.06° in the range of 30–708 and with $Cu_{K\alpha}$ radiation (λ=0.15405 nm). The samples were examined to obtain size/shape images of nanostructured materials using a Philips Tecnai G2 F20 high-resolution transmission electron microscopy (HRTEM). X-ray photoelectron spectroscopy (XPS) was conducted on a Thermo VG Scientific ESCALAB 250 spectrometer with a monochromated $Al_{K\alpha}$ excitation source. A vibrating sample magnetometer (VSM, Lake Shore 7404) was used to characterize the magnetic properties of as-synthesized samples. The magnetic hysteresis curve was obtained by changing magnetic field between +17000 and @17000 Oe.

Electrochemical Measurements

All electrolysis measurements were conducted on a CHI650 Electrochemical work station in O_2-saturated 1 M KOH solution. Typically, a mixture of ultrapure water (715 μL), ethanol (245 μL), and Nafion solution (40 μL), catalysts (4 mg) and acetylene black (1 mg) was dispersed by sonication for 30 min. Then 10 μL of homogeneous catalyst ink was dropped on to a polished glassy carbon electrode with a diameter of 3 mm (0.57 mg cm^{-2}) as the working electrode. Platinum wire was used as the counter electrode and an Hg/HgO electrode as the reference electrode. Linear scan voltammetry was performed at a scan rate of 5 $mV \cdot s^{-1}$ to obtain polarization curves. During the test, the system was continuously purged with high-purity O_2. All of the potentials were calibrated to the RHE by adding a value of 0.924 V ($E_{RHE}=E_{Hg/HgO}+ (0.059\times pH) + 0.098$). The OER equilibrium potential (E_0) is 1.23 V vs RHE. The overpotential is the potential difference between E_{RHE} and E_0.

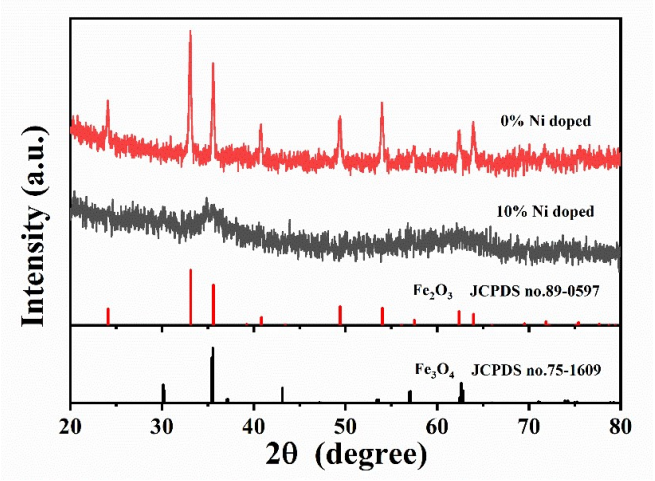

Fig. S1 The XRD spectra of 0% and 10% Ni-doped iron oxide precursor after solvothermal.

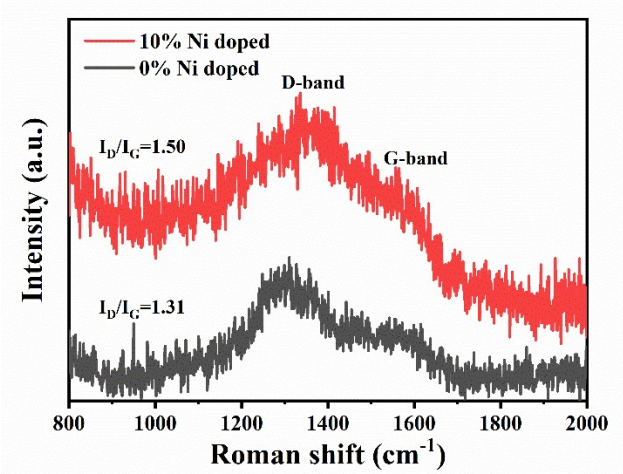

Fig. S2 Roman spectrum for $(Fe_1Ni_0)_4N$ and $(Fe_{0.90}Ni_{0.10})_4N$.

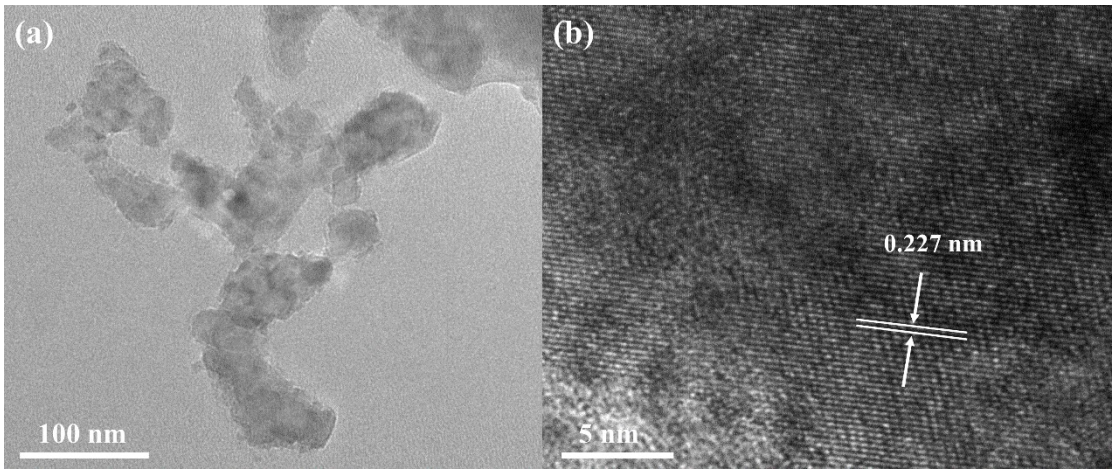

Fig. S3 (a) Low-magnification TEM images (b) High-magnification TEM images for $(Fe_1Ni_0)_4N$ samples.

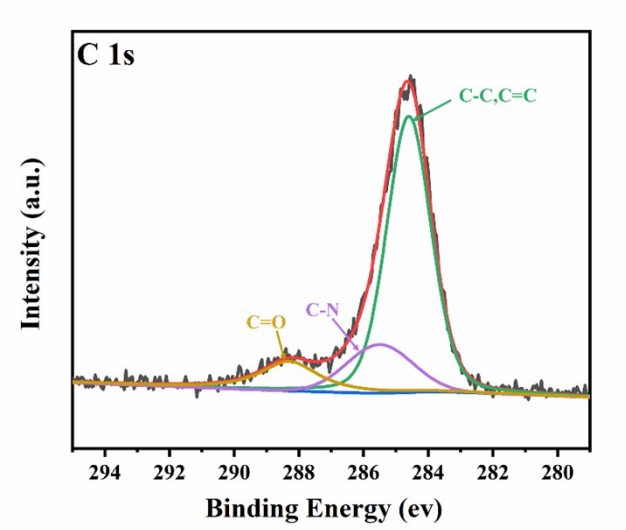

Fig. S4 High-resolution XPS spectra of C 1s for $(Fe_{0.90}Ni_{0.10})_4N$.

Table S1. The element contents for $(Fe_1Ni_0)_4N$ and $(Fe_{0.90}Ni_{0.10})_4N$ samples from XPS results.

Samples/element content	N 1s	O 1s	C 1s	Fe 2p	Ni 2p
$(Fe_1Ni_0)_4N$	3.32%	26.03%	67.67%	2.98%	--------
$(Fe_{0.90}Ni_{0.10})_4N$	3.72%	29.5%	60.9%	5.34%	0.54%

Table S2 Magnetic parameters of products with different Ni doping concentrations

The doping concentration of Ni	M_s (emu/g)	H_c (G)	M_r (emu/g)
0%	142.89	129.07	11.01
3%	168.15	98.49	10.65
5%	165.34	106.75	11.43
7%	157.06	113.95	11.60
10%	153.02	115.16	10.97
12%	113.53	151.89	11.49
15%	45.55	285.15	9.42

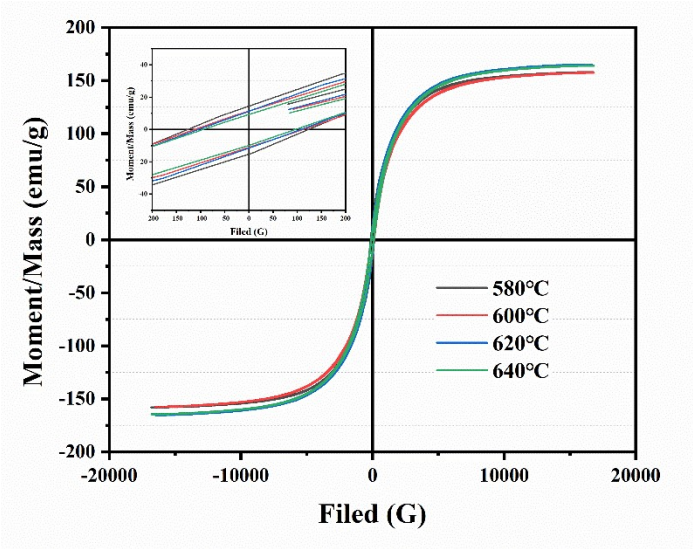

Fig. S5 Magnetic hysteresis loops at room temperature: samples with 5% Ni-doped prepared at different nitriding temperatures

Table S3. Comparison of the electrocatalytic performance of OER electrocatalysts reported recently, η_{10} is the overpotential at the current density of 10 mA cm^{-2}.

Catalyst	η_{10}	Tafel slope	Electrolyte	Ref.
$(Fe_{0.90}Ni_{0.10})_4N$	292 mV	29	1 M KOH	This work
Fe_{NP}@Fe-N-C	340 mV	216	0.1 M KOH	[1]
Fe_2P/Fe_4N@C	410 mV	177	1 M KOH	[2]
Ni_2Fe_2N@N-CS	264 mV	47.8	1 M KOH	[3]
Ni_3FeN/N-G	320 mV	45	1 M KOH	[4]
Ni_3FeN-NPs	280 mv	46	1 M KOH	[5]
IrO_2	340 mV	61	1 M KOH	[4]

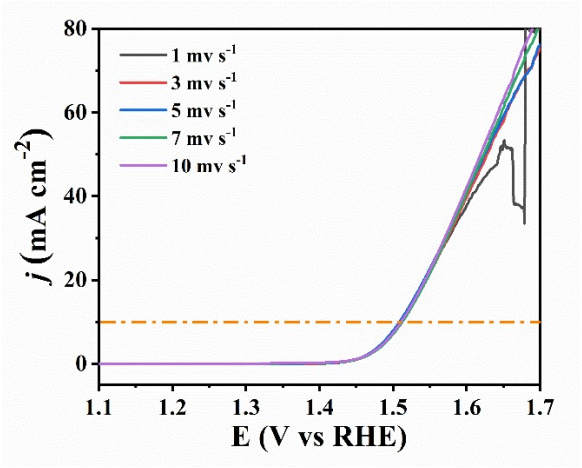

Fig. S6 Polarization curves recorded at different scan rate of the $(Fe_{0.90}Ni_{0.10})_4N$ in 1.0 M KOH.

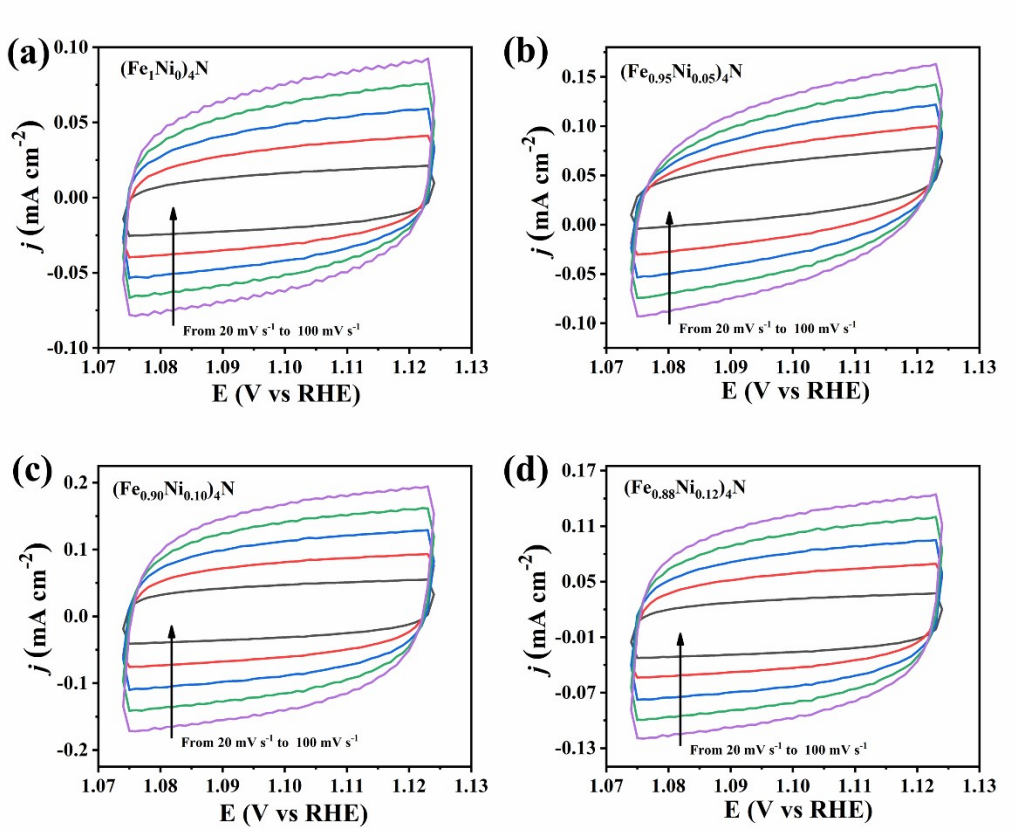

Fig. S7 CV curves of samples prepared with different nickel doping concentrations recorded at different scanning rates ranging from 20 to 100 mV s^{-1} with an interval point of 20 mV s^{-1}.

References

[1] C. Yang, S. Shang, Q. Gu, J. Shang, X.-y. Li, Metal-organic framework-derived carbon nanotubes with multi-active Fe-N/Fe sites as a bifunctional electrocatalyst for zinc-air battery. J. Energy Chem. 2022, 66, 306–31.

[2] X. Fan, F. Kong, A. Kong, A. Chen, Z. Zhou, Y. Shan, Covalent Porphyrin Framework-Derived Fe_2P@Fe_4N-Coupled Nanoparticles Embedded in N-Doped Carbons as Efficient Trifunctional Electrocatalysts. ACS Appl. Mater. Interfaces2017, 9, 32840−32850.

[3] H. W. Choia, D. I. Jeong, S. B. Kwon, S. Woo, J. Kim, J. H. Kim, W. S. Yang, B. Lim, B. K. Kang, D. H. Yoon, Nickel-Iron nitrides and alloy heterojunction with amorphous N-doped carbon Shell: High-efficiency synergistic electrocatalysts for oxygen evolution reaction. Appl. Surf. Sci. 2021, 566, 150706.

[4] S. Zhao, M. Li, M. Han, D. Xu, J. Yang, Y. Lin, N.-E. Shi, Y. Lu, R. Yang, B. Liu, Z. Dai, J. Bao, Defect-Rich Ni_3FeN Nanocrystals Anchored on N-Doped Graphene for Enhanced Electrocatalytic Oxygen Evolution. Adv. Funct. Mater. 2018, 28, 1706018.

[5] X. Jia, Y. Zhao, G. Chen, L. Shang, R. Shi, X. Kang, G. I. N. Waterhouse, L.-Z. Wu, C.-H. Tung, T. Zhang, Ni_3FeN Nanoparticles Derived from Ultrathin NiFe-Layered Double Hydroxide Nanosheets: An Efficient Overall Water Splitting Electrocatalyst. Adv. Energy Mater. 2016, 6, 1502585.